

Power consumption reduction scheme of magnetic microactuation using electroplated Cu–Ni nanocomposite

Yu Wen Huang, Tzu-Yuan Chao, C. C. Chen, and Y. T. Cheng

Citation: [Applied Physics Letters](#) **90**, 244105 (2007); doi: 10.1063/1.2748301

View online: <http://dx.doi.org/10.1063/1.2748301>

View Table of Contents: <http://scitation.aip.org/content/aip/journal/apl/90/24?ver=pdfcov>

Published by the [AIP Publishing](#)

Articles you may be interested in

[Electroplating hard magnetic SmCo for magnetic microactuator applications](#)

J. Appl. Phys. **109**, 07A766 (2011); 10.1063/1.3565414

[Thin film SmCo magnets for use in electromagnetic microactuators](#)

J. Appl. Phys. **99**, 08N304 (2006); 10.1063/1.2176390

[Electroplated CoFe thin films for electromagnetic microactuators](#)

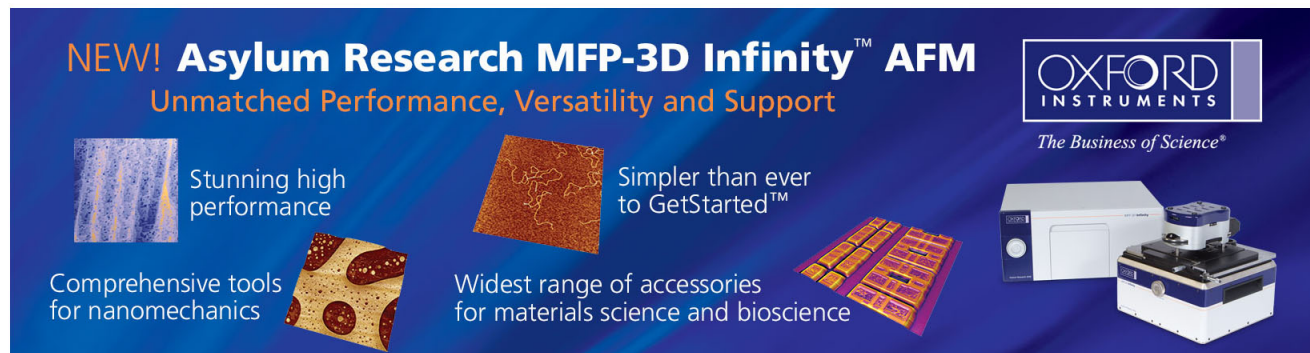
J. Appl. Phys. **99**, 08M308 (2006); 10.1063/1.2176239

[Morphological and magnetic properties of carbon–nickel nanocomposite thin films](#)

J. Appl. Phys. **97**, 044313 (2005); 10.1063/1.1852702

[Magnetic exchange effects in a nanocomposite Ni/NiO film](#)

J. Appl. Phys. **91**, 7233 (2002); 10.1063/1.1447193

The advertisement features a dark blue background with white and orange text. At the top left, it reads 'NEW! Asylum Research MFP-3D Infinity™ AFM' in large white letters, followed by 'Unmatched Performance, Versatility and Support' in orange. To the right is the Oxford Instruments logo, which includes the text 'OXFORD INSTRUMENTS' and the tagline 'The Business of Science®'. Below the text are several images: a textured surface, a circular pattern, a grid of small squares, and the physical AFM instrument. Text boxes describe the instrument's capabilities: 'Stunning high performance', 'Simpler than ever to GetStarted™', 'Comprehensive tools for nanomechanics', and 'Widest range of accessories for materials science and bioscience'.

Power consumption reduction scheme of magnetic microactuation using electroplated Cu–Ni nanocomposite

Yu Wen Huang, Tzu-Yuan Chao, C. C. Chen, and Y. T. Cheng^{a)}

Microsystems Integration Laboratory, Department of Electronics Engineering, National Chiao Tung University, Hsinchu, 300 Taiwan, Republic of China

(Received 7 March 2007; accepted 13 May 2007; published online 13 June 2007)

This letter presents a power consumption reduction scheme of magnetic microactuation using Cu–Ni nanocomposite film which is electroplated in alkaline noncyanide based Ni colloidal copper plating solution at 40 °C. The superconducting quantum interference device magnetometer measurements show that Cu film is modified from diamagnetism to ferromagnetism via the incorporation of Ni ferromagnetic nanoparticles into itself to form a Cu–Ni nanocomposite film. A magnetic microactuator made of the nanocomposite can have about 9% performance improvement in terms of actuation enlargement. In other words, the coil made of the Cu–Ni nanocomposite can exhibit better power efficiency for the same output displacement. © 2007 American Institute of Physics. [DOI: 10.1063/1.2748301]

Magnetic microactuators are typically designed with an inductive microcoil driven by an electrical current under a magnetic field to generate electromagnetic force (EMF) for magnetic microactuation.^{1,2} In comparison with the other types of microactuators driven by the source of electrostatic, piezoelectric, or electrothermal force, the actuator with EMF can exhibit the characteristics of low driving voltage and large output force, which are good for miniaturization.^{3–5} Besides, magnetic microactuators can be fabricated using complementary metal-oxide semiconductor (CMOS)-compatible thin film processes. Thus, these excellent characteristics make magnetic microactuators fascinating for microelectromechanical systems (MEMS) applications. A variety of magnetic microactuators has been designed and fabricated.^{6–8} Recent research objectives in the development of magnetic microactuator are focused on power consumption reduction for portable microsystem applications.^{9,10} According to the Lorentz force law, the induced EMF exerted on the point *P* of the coil shown in Fig. 1 is as follows:

$$\mathbf{F} = I d\hat{l} \times \mathbf{B}, \quad (1)$$

where \mathbf{F} , I , $d\hat{l}$ and \mathbf{B} are the magnetic force, electric current, unit length, and magnetic flux density of the coil at point *P*, respectively. Since the EMF is proportional to the strength of both magnetic field and electric current driven in an inductive coil, it has been a challenge to have a large EMF in a microactuator where the field and current input are limited in a finite volume. In addition, increasing electric current to enlarge EMF is not a considerate approach for low-power applications due to the formation of larger Joule heating loss which is not power efficient.¹¹ In order to resolve this problem, most research efforts have been put on the deposition of magnet with high saturated magnetization (M_s), such as NiFe, CoNbZr, and SrO₆Fe₂O₃ for creating large magnetic field.¹² In this letter, we will present a distinct approach to enhance EMF which can combine with the aforementioned approach to realize power-efficient magnetic microactuation.

In general, the magnetic field at the point *P* in Fig. 1 not only can come from the bias magnet underneath the coil but also can be contributed by the coil as long as the coil is made

of magnetic material that can be magnetized by the bias magnet. Under the same current input, the induced EMF of a magnetic microactuator driven by a magnetic coil can be larger than that of the microactuator with the same design but driven by a nonmagnetic coil because the applied magnetic flux density at the point *P* is further intensified via the introduction of magnetization inside the coil. Although the simplest way to realize the introduction is to utilize a conductive magnetic material for the coil fabrication such as a NiFe Permalloy, inevitable high resistivity ($\sim 1.5 \times 10^{-5} \Omega \text{ cm}$) still results in large Joule heating loss which deteriorates the performance of magnetic microactuator for low-power applications.

Previously, metal-based nanocomposites were synthesized and proposed for low-power MEMS fabrication.^{13,14} The physical properties of metal film can be modified for special applications via the secondary phase and size effects. For example, the incorporation of carbon nanotubes into Ni matrix makes the composite material fascinating for low-power electrothermal microactuator fabrication.¹³ An on-chip inductor made of Cu–CoFe₂O₄ nanocomposite could have high *Q* and large inductance performance for low-power radio frequency integrated circuits.¹⁴ According to the previous investigations on the electrical conductivity of metal-based nanocomposite,¹³ the Maxwell-Wagner equation¹⁵ based on the model of two-phase random network can provide good estimation and the conductivity can be calculated as follows:

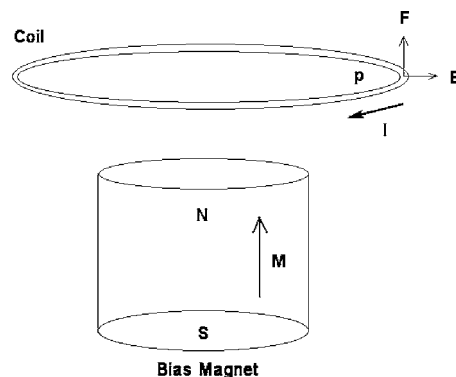


FIG. 1. General scheme of magnetic actuation.

^{a)}Electronic mail: ytcheng@mail.nctu.edu.tw

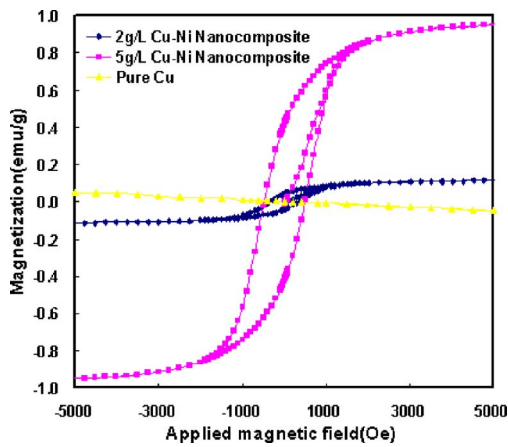


FIG. 2. SQUID measurements of pure Cu and Cu–Ni nanocomposites plated in a bath added with 2 and 5 g/l Ni nanopowders, respectively.

$$k_c = k_m \frac{1 + 2V_f(1 - k_m/k_d)/(1 + 2k_m/k_d)}{1 - V_f(1 - k_m/k_d)/(1 + 2k_m/k_d)}, \quad (2)$$

where k_c , k_d , and k_m are the electrical conductivities of the composite film, embedded secondary phase, and metal matrix, respectively, and V_f is the volume fraction of the embedded secondary phase. Meanwhile, from the rule of mixture,¹⁶ the induced magnetic moment of composite (M_i) inside a Cu matrix due to the incorporation of magnetic particles into Cu matrix can be simply estimated based on the intrinsic induced magnetic moment and the weight ratio of the magnetic particle and Cu.

$$M_i = M_c W_c + M_m W_m, \quad (3)$$

where W_m , W_c , M_m , and M_c represent the weight percents and induced magnetic moment of the incorporated particle and metal matrix, respectively. From Eqs. (1)–(3), the correlation in terms of power consumption between the magnetic microactuators using pure Cu and nanocomposite coils for the same output force, respectively, can be calculated as follows:

$$P_{\text{composite}} = P_c \left(\frac{H_{\text{applied}}}{H_{\text{applied}} + M_i} \right)^2 \frac{k_m}{k_c}, \quad (4)$$

where H_{applied} is the magnetic field strength coming from the magnet underneath the coil and $P_{\text{composite}}$ and P_c are the power consumptions of the magnetic microactuators using nanocomposite and pure Cu coils, respectively. Adequately choosing a composite material with large M_i and k_c can effectively reduce the power consumption of magnetic actuators. Therefore, a Cu–Ni nanocomposite is proposed and synthesized here to realize the goal of low-power magnetic microactuation. Instead of the aforementioned CoFe_2O_4 or other ferromagnetic materials, Ni powders are chosen for their having a nice ratio of k_m to k_c for better power efficiency since Ni has lower electrical resistivity than NiFe.

Here, ~ 50 nm Ni nanopowders are chosen to mix with a copper plating solution to form a colloidal bath for the Cu–Ni nanocomposite film synthesis. Isopropyl alcohol (IPA) is utilized here as a dispersant for the separation of Ni nanoparticles in the solution. Once the Ni nanoparticles are added into IPA, a colloidal solution with well-dispersed Ni particles can be formed using mechanical stirring and ultrasonication. Before putting the colloidal solution into Cu plating bath, the solution is first added with the proper amount of

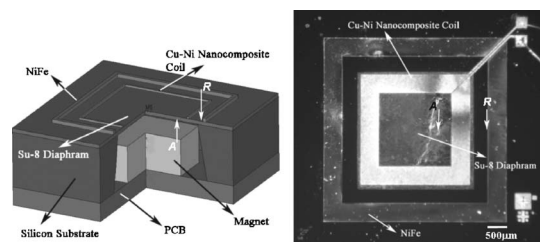


FIG. 3. (a) Diagram of magnetic microactuation structure designed for the low-power scheme verification and (b) the top view of as-fabricated SU-8 diaphragm with magnetic Cu–Ni nanocomposite coil.

water then heated up to 40°C to drive IPA out of the water since IPA would block Cu seed layer surface for plating. Here, instead of conventional sulfuric Cu plating solution, the commercial alkaline noncyanide based copper plating solution¹⁷ is chosen for the nanocomposite synthesis because the Ni particles will chemically react with acidic sulfuric copper plating solution. The reaction causes little Ni nanopowder incorporation in Cu matrix. By adjusting the amount of Ni nanoparticles being added into the solution, Cu–Ni magnetic nanocomposites with different Ni incorporations can be synthesized. The composite plating rate is controlled at $\sim 0.2 \mu\text{m}/\text{min}$. While Cu is plated, well-dispersed Ni nanopowders are engulfed in Cu matrix to form magnetic Cu–Ni nanocomposite. Figure 2 shows superconducting quantum interference device (SQUID) measurement. The magnetic property of Cu film is modified from diamagnetism to ferromagnetism via the incorporation of Ni nanoparticles and the M_s of Cu–Ni nanocomposite increases with the amount of Ni nanoparticles being added into plating bath.

A microstructure shown in Fig. 3 is fabricated for low-power scheme verification. The fabrication begins with $0.6 \mu\text{m}$ thermal oxide deposition, followed by $0.6 \mu\text{m}$ low-stress nitride deposition on a p -type silicon (p -Si) substrate. A diaphragm area driven by inductive coil is then defined and patterned from the back side of the silicon substrate via chemical wet etching using KOH. A $5 \mu\text{m}$ thick SU-8 film is then spun onto the etched substrate to form the actuated diaphragm. After the diaphragm fabrication, a sandwich layer of Ti (10 nm)/Cu (120 nm)/Ti (5 nm) is evaporated and patterned to serve as a seeding layer for electroplating. The inductive coil is patterned then electroplated in the aforementioned Cu–Ni colloidal solution added with 2 g/l Ni nanopowders to form a $2 \mu\text{m}$ thick magnetic Cu–Ni nanocomposite coil. During the plating, the wafer is placed in a vertical fashion inside the bath with mechanical stirring at 120 rpm and the bath temperature is kept at 40°C . In order to ensure a uniform magnetic field laterally applied on the inductive coil, other conventional photolithography and electroplating processes¹⁸ are performed for NiFe Permalloy ring fabrication. Finally, the silicon substrate is then bonded with a print circuit board (PCB) board using ALTECO adhesive to form a microcavity inside on which a 0.02 T magnet is mounted, as shown in Fig. 3(a). Figure 3(b) shows the top view of as-fabricated device.

Figure 4 shows the vertical displacements of the SU-8 diaphragms actuated by Cu and Cu–Ni nanocomposite coils, respectively. The displacement measurement is performed using an optical interferometer with subnanometer vertical resolution and calculated to be equal to the height difference of the point A shown in Fig. 3(a) while the coil is applied with and without an electric current input. Here, the height of

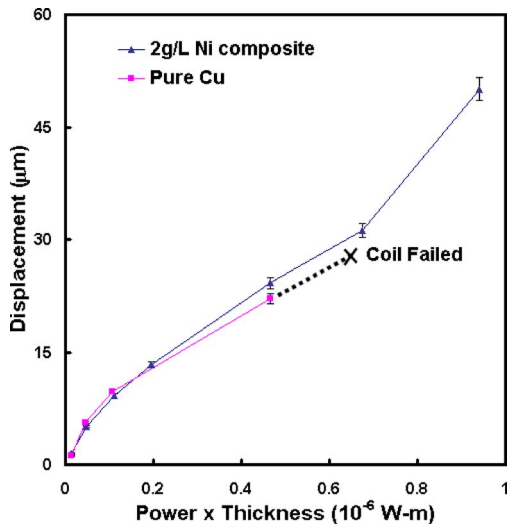


FIG. 4. Vertical displacement of SU-8 diaphragms vs the normalized input to the driving coils, which are made of Cu and Cu–Ni nanocomposite, respectively.

point *A* is referenced to a fixed point, called *R*, under which silicon substrate is not removed. Due to process variation, the power consumption is normalized by the thickness of inductive coil for fair comparison. From the measurement, it is found that, under the same input, the diaphragm driven by Cu–Ni composite coil can have a larger displacement while the displacement exceeds 10 μm . Under the same input of $4.67 \times 10^{-7} \text{ W m}$, the diaphragm driven by pure Cu coil has 22 μm vertical displacement which is 2 μm less than that driven by Cu–Ni nanocomposite coil. In other words, the coil made of magnetic Cu–Ni nanocomposite can exhibit better power efficiency for the same displacement. In addition, Fig. 4 also shows that Cu–Ni nanocomposite coil can make the SU-8 diaphragm have much larger displacement than the one made of pure Cu before the coils are failed.

According to Eq. (4), the power reduction scheme can be realized as long as the ratio of $P_{\text{composite}}/P_c$ is smaller than 1 and the proposed Cu–Ni nanocomposite is just fit into the role. With the assumption of isotropic magnetization of spherical Ni particles inside Cu matrix, Eq. (4) can be simplified as follows:

$$P_{\text{composite}}/P_c = \left(\frac{\mu_{r,\text{Cu}}}{\mu_{r,\text{composite}}} \right)^2 \frac{k_m}{k_c}. \quad (5)$$

The $\mu_{r,\text{composite}}$ can be calculated based on the Bruggeman approach¹⁹ as follows since the added Ni particle size is very small:

$$\mu_{r,\text{composite}} = \mu_{\text{Cu}} + (1 - f_{\text{Cu}}) \frac{\alpha_h^{\text{Ni/Cu}}}{1 - (1 - f_{\text{Cu}})(\alpha_h^{\text{Ni/Cu}}/3\mu_{r,\text{Cu}})}, \quad (6)$$

$$\alpha_h^{\text{Ni/Cu}} = 3\mu_{r,\text{Ni}} \frac{\mu_{r,\text{Ni}} - \mu_{r,\text{Cu}}}{\mu_{r,\text{Ni}} + 2\mu_{r,\text{Cu}}}, \quad (7)$$

where f_{Cu} is the volume ratio of Cu in the composite, $\alpha_h^{\text{Ni/Cu}}$ is the magnetizability density, and $\mu_{r,\text{Cu}}$ and $\mu_{r,\text{Ni}}$ are relative permeabilities of Cu and Ni, respectively. For the case of Cu–Ni nanocomposite, $\mu_{r,\text{Cu}}$ and $\mu_{r,\text{Ni}}$ are 0.999 and 9,²⁰ respectively. The $\mu_{r,\text{composite}}$ can be modified from 1.21 to

2.46 while the volume fraction of embedded Ni particles is changed from 1% to 5%. Meanwhile, the value of k_m/k_c shown in Eq. (3) is also changed from 1.015 to 1.079. Thus, $P_{\text{composite}}/P_c$ will theoretically fall in a range of 0.18 to 0.69. More than 18% power reduction could be realized. Nevertheless, it is noted that the calculation of k_m/k_c ratio is simply based on the electrical conductivities of Cu and Ni films. Since the electrical conductivity of metal particle could be smaller than that of metal film²¹ and would result in a larger k_m/k_c ratio. Meanwhile, the size of Ni particles used here is about 50 nm in which the coercive force is around 250 Oe Ref. 22 and is comparable with the magnetic field intensity of the bias magnet that we use in the device. Only part of Ni particles can be fully magnetized by the bias magnet. Therefore, it is reasonable that only 9% performance improvement has been observed so far. The characterizations of Cu–Ni nanocomposites and the Ni nanoparticle size and spin dependent scattering effects on the electrical conductivity of the composite are still required for further optimization for low-power magnetic microactuation design.

In summary, this letter presents a power consumption reduction scheme and verification using Cu–Ni nanocomposite. The approach can lead the way to further saving operational power in the present magnetic microactuator designs. The Cu–Ni nanocomposite and related low temperature fabrication process also show the potential applications for MEMS fabrications due to its CMOS process compatibility.

This work was supported by the NSC 95-2220-E-009-021 project and in part by MediaTek Research Center at National Chiao Tung University.

¹J. H. Ku, J. O. Chan, and Y. S. Sik, Proc. SPIE **3990**, 272 (2000).

²S. Bhansali, L. A. Lei, B. R. Zmood, P. E. Jones, and D. K. Sood, J. Microelectromech. Syst. **9**, 245 (2000).

³J. Singh, A. Agarwal, and M. Soundarapandian, Thin Solid Films **504**, 64 (2006).

⁴P. C. Shiang and W. Hsu, J. Micromech. Microeng. **7**, 7 (1997).

⁵D. Damjanovic, K. G. Brooks, A. Kholkin, M. Kohli, T. Maeder, P. Murali, and N. Setter, Mater. Res. Soc. Symp. Proc. **360**, 429 (1995).

⁶C. T. Pan and S.-C. Shen, J. Magn. Magn. Mater. **285**, 422 (2005).

⁷C. H. Ahn and M. G. Allen, J. Micromech. Microeng. **3**, 37 (1993).

⁸D. de Bhaillis, C. Murray, M. Duffy, J. Alderman, G. Kelly, and S. C. Mathuna, Sens. Actuators, A **81**, 285 (2000).

⁹I.-J. Cho, T. Song, S.-H. Baek, and E. Yoon, IEEE Trans. Microwave Theory Tech. **53**, 2450 (2005).

¹⁰D. Rajesh and L. Amit, J. Microelectromech. Syst. **14**, 488 (2005).

¹¹B. Wagner, W. Benecke, G. Engelmann, and J. Simon, Sens. Actuators, A **32**, 598 (1992).

¹²H. J. Cho and C. H. Ahn, J. Microelectromech. Syst. **11**, 78 (2002).

¹³G.-R. Shen, Y. T. Cheng, and L.-N. Tsai, IEEE Trans. Nanotechnol. **4**, 539 (2005).

¹⁴T.-Y. Chao and Y. T. Cheng, Proceedings of the IEEE Conference on Nanotechnology, 2006, p. 810.

¹⁵D. G. Han and G. M. Choi, Solid State Ionics **106**, 71 (1998).

¹⁶B. D. Cullity, *Introduction to Magnetic Materials* (Addison-Wesley, New York, 1973), p. 191.

¹⁷M. Schlesinger and M. Paunovic, *Modern Electroplating*, 4th ed. (Wiley, New York, 2000), p. 104.

¹⁸M.-C. Cheng, W.-S. Huang, and S. R.-S. Huang, J. Micromech. Microeng. **14**, 859 (2004).

¹⁹A. Lakhtakia and T. G. Mackay, AEU, Int. J. Electron. Commun. **58**, 1 (2004).

²⁰N. J. Tang, W. Zhong, W. Liu, H. Y. Jiang, X. L. Wu, and Y. W. Du, Nanotechnology **15**, 1756 (2004).

²¹S. Singamaneni and V. Bliznyuk, Appl. Phys. Lett. **87**, 162511 (2005).

²²Y.-W. Du, M.-X. Xu, J. Wu, Y.-B. Shi, H.-X. Lu, and R.-H. Xue, J. Appl. Phys. **70**, 5903 (1991).